ANTIOXIDANTS & REDOX SIGNALING
Volume 21, Number 10, 2014

DOI: 10.1089/ars.2013.5446

ORIGINAL RESEARCH COMMUNICATION

The Oxidation States of DJ-1 Dictate the Cell Fate in Response to Oxidative Stress Triggered by 4-HPR: Autophagy or Apoptosis?

Ji Cao,* Meidan Ying,* Nan Xie, Guanyu Lin, Rong Dong, Jun Zhang, Hailin Yan, Xiaochun Yang, Qiaojun He, and Bo Yang

Abstract

Aim: Chemotherapy-induced reactive oxygen species (ROS) not only contribute to apoptosis, but also trigger autophagy. Since autophagy is reported to protect cancer cells from apoptosis, this weakens the therapeutic effect of chemotherapy. This study aimed at identifying the key molecules that determine the cellular response to ROS and, therefore, provide better strategies to increase chemotherapeutic efficiency. ***Results:*** Increasing concentrations of N-(4-hydroxyphenyl) retinamide (4-HPR)-treatment pushed autophagy down to apoptosis in a dose-dependent manner, and 4-HPR-induced ROS contribute to this process. Since we found that ASK1-regulated JNK1 and p38 are responsible for 4-HPR-induced autophagy and apoptosis, respectively, we further utilized co-immunoprecipitation followed by liquid chromatography-tandem mass spectrometry analysis to identify proteins that specifically bind to ASK1 under different oxidative states. Of note, DJ-1, a crucial antioxidant protein, was identified. Interestingly, DJ-1 functions as a redox sensor that senses ROS levels and determines the cellular response to 4-HPR: Under mild oxidative stress, moderate oxidation of DJ-1 is recruited to inhibit the activity of ASK1 and maintain cell viability by activating autophagy; under a lethal level of oxidative stress, excessive oxidized DJ-1 dissociates from ASK1 and activates it, thereby initiating p38 activation and enabling the cells to commit to apoptosis. Moreover, the depletion of DJ-1 increases the sensitivity of tumor cells to 4-HPR both *in vitro* and *in vivo*. ***Innovation:*** Our results reveal that the different oxidation states of DJ-1 function as a cellular redox sensor of ROS caused by 4-HPR and determine the cell fate of autophagy or apoptosis. Moreover, the results suggest that DJ-1 might be a potent therapeutic target for cancer treatment. ***Conclusion:*** ROS-mediated changes in the oxidation state of DJ-1 are involved in 4-HPR's effect on pushing autophagy down to apoptosis. Consequently, this change mediates ASK1 activation by regulating DJ-1-ASK1 complex formation and determines the cell fate of autophagy or apoptosis. *Antioxid. Redox Signal.* 21, 1443–1459.

Introduction

Macroautophagy (hereafter referred to as ''autophagy'') and apoptosis are two distinct and interconnected cell fates that play critical roles in response to chemotherapies. Low-intensity stress caused by chemotherapy leads to the induction of autophagy, which, in turn, selectively recycles long-lived proteins and defective organelles. With an increase in stress, apoptosis begins to occur. Although increased formation of autophagosomes can also be associated with autophagic cell death, it is generally considered that autophagy and apoptosis are antagonistic, and autophagy is a major protective pathway which tends to inhibit apoptosis in response to chemotherapies (10, 26). One potential stimulus of both autophagy and apoptosis is reactive oxygen species (ROS), which has a functional duality that is also apparent in various cancer cells (2, 3). For example, ROS initially improve tumor promotion; however, if the ROS are overwhelmed, apoptosis can be initiated (15). In addition, many stimuli that induce ROS generation also drive

Zhejiang Province Key Laboratory of Anti-Cancer Drug Research, Department of Pharmacology, College of Pharmaceutical Sciences, Zhejiang University, Hangzhou, China.
*These authors contributed equally to this work.

Innovation

DJ-1 is a multifunctional oxidative stress response protein that has been intensely studied in neurons; however, its role in cancer is poorly understood. Our results support a model (Fig. 8) in which the oxidation states of DJ-1 function as a redox sensor that controls the cellular response to N-(4-hydroxyphenyl) retinamide (4-HPR)-driven reactive oxygen species *via* its interaction with ASK1. Of note, the depletion of DJ-1 increases the sensitivity of tumor cells to 4-HPR both *in vitro* and *in vivo*. These findings enrich our understanding of the cellular regulation of antioxidative and redox signaling and indicate that targeting DJ-1 may be a useful strategy in cancer chemotherapeutics.

autophagy and/or apoptosis, including nutrient starvation, exposure to mitochondrial toxins, hypoxia, and oxidative stress. Hence, multiple connections should exist between ROS, autophagy, and apoptosis, and whether cells are committed to death or life most likely depends on small shifts in the particular circumstances. Therefore, the identification of switching molecules that determine the cellular response to ROS is now receiving considerable attention.

Of the many intracellular signaling pathways involved in oxidative stress responses, the mitogen-activated protein kinase (MAPK) cascade is one of the most important signaling pathways. c-Jun N-terminal kinases (JNKs) and p38 MAPKs are preferentially activated by environmental stress; therefore, they are often grouped together and referred to as stress-activated protein kinases (SAPKs). Although the idea that SAPKs often have similar physiological roles in stress-induced apoptosis is still generally accepted, recent studies suggest that JNKs may be more likely to induce autophagy compared with p38. For example, the activation of JNKs, up-regulation of ATG5, and induction of autophagic cell death observed in H-ras (V12)-transfected fibroblasts were rescued by the inhibition of MKK7 but not of MKK4 (4). Consistent with this finding, JNKs also mediate etoposide-caused autophagic death in Bax/Bak double-knockout MEFs. In fact, the deletion of the JNK upstream kinases SEK1 and MKK7 in MEFs restored cell viability after treatment with etoposide (42). Given that MKK4, the co-upstream kinase of JNKs and p38, has no effect on the activation of autophagy, it is possible that only JNK signaling plays a key role in the initiation of autophagy. In view of this, we propose that JNKs and p38 may have diverse roles in autophagy and apoptosis induction, respectively. Thus, the major question is how cells selectively activate SAPKs and determine the appropriate response to ROS.

Apoptosis signal-regulating kinase 1 (ASK1) is a MAP kinase kinase kinase (MAP3K) that activates both JNK and p38 signaling and has been demonstrated to function as a redox sensor (36). For example, under conditions in which there is no oxidative stress, the antioxidant protein thioredoxin (Trx) forms a complex with ASK1 and inhibits its kinase activity (39). Under oxidative stress conditions, the oxidized form of Trx is released from ASK1, and activated ASK1 directly phosphorylates and activates MKK4/7 and MKK3/6, leading to JNKs and p38 activation. It appears as though the ASK1-Trx complex can sense the existence of redox, but whether it can sense the extent of oxidative stress is not known. Moreover, very little is known about the hierarchy of events involved in this process, particularly those related to how ASK1 sense the extent of oxidative stress and finely regulates the induction of autophagy and apoptosis, respectively. Considering that the regulation of ASK1 activation has been revealed mainly through ASK1-binding proteins, we hypothesize that the construction of a suitable cellular model with serial inducible redox levels will enable the identification of additional regulators which finely inhibit or activate ASK1.

The cancer chemopreventive and therapeutic retinoid N-(4-hydroxyphenyl) retinamide (4-HPR) has been widely studied in both preclinical models and clinical trials of cancer prevention (27, 37, 49, 54). Data from our group and others indicate that the generation of ROS mediates reversible 4-HPR cytotoxicity in cancer cells (7, 12) and that both autophagy and apoptosis can be induced by 4-HPR (13, 25, 30). Thus, we aimed at determining the key partner of ASK1 that provides the connection between ROS and the 4-HPR's effect on pushing autophagy down to apoptosis. In this study, we demonstrated that p38 and JNK1 serve as two different downstream signals that mediate the induction of apoptosis and autophagy, respectively, and ASK1 forms a complex with DJ-1 in response to 4-HPR-triggered ROS. The interaction between ASK1 and DJ-1 depends on the level of ROS. Further studies indicated that the depletion of DJ-1 increases the sensitivity of tumor cells to 4-HPR both *in vitro* and *in vivo.* Collectively, our results support a model in which DJ-1 senses the extent of oxidative stress caused by chemotherapy, thereby dictating the cell fate. In addition, our results suggest that DJ-1 might be a potent therapeutic target for cancer.

Results

4-HPR pushes autophagy down to apoptosis in a concentration threshold-dependent manner both in vitro *and* in vivo

Several recent reports showed that both autophagy and apoptosis can be induced by 4-HPR treatment (13, 46). Interestingly, when we focused on the hypoxia-induced resistance of HeLa cells to 4-HPR (30), we occasionally observed that 4-HPR pushed autophagy down to apoptosis. In the present study, a similar phenomenon was also observed in several cancer cells. As illustrated in Figure 1A, a concentration-dependent selective increase in LC3-II [a widely accepted autophagy marker (19, 32)] was observed in HeLa cells that were treated with 4-HPR for 24 h. Acridine orange (AO) staining, MDC staining, and GFP-LC3 transfection assays were further performed to visualize autophagosome formation in the cells. In agreement with the results in Figure 1A, less autophagosome accumulation was observed in control cells, whereas accumulation increased after treatment with 5 and 10 μM 4-HPR (Fig. 1B). Electron microscopic observations also revealed that 4-HPR treatment led to the accumulation of autophagosomes in HeLa cells, as numerous autophagic vacuoles, empty vacuoles, and secondary lysosomes were observed (Fig. 1B, bottom two panels). Of note, although a significant increase in autophagy was noted under treatment with both 5 and 10 μM 4-HPR, the cleaved fragment of PARP [a classic apoptosis marker (3), Fig. 1A] and condensation of chromatin (red arrow, Fig. 1B) were only observed under treatment with 10 μM 4-HPR. Similar results were also observed in human osteosarcoma MG-63, colon cancer HCT116, hepatocellular carcinoma HepG2, and oral

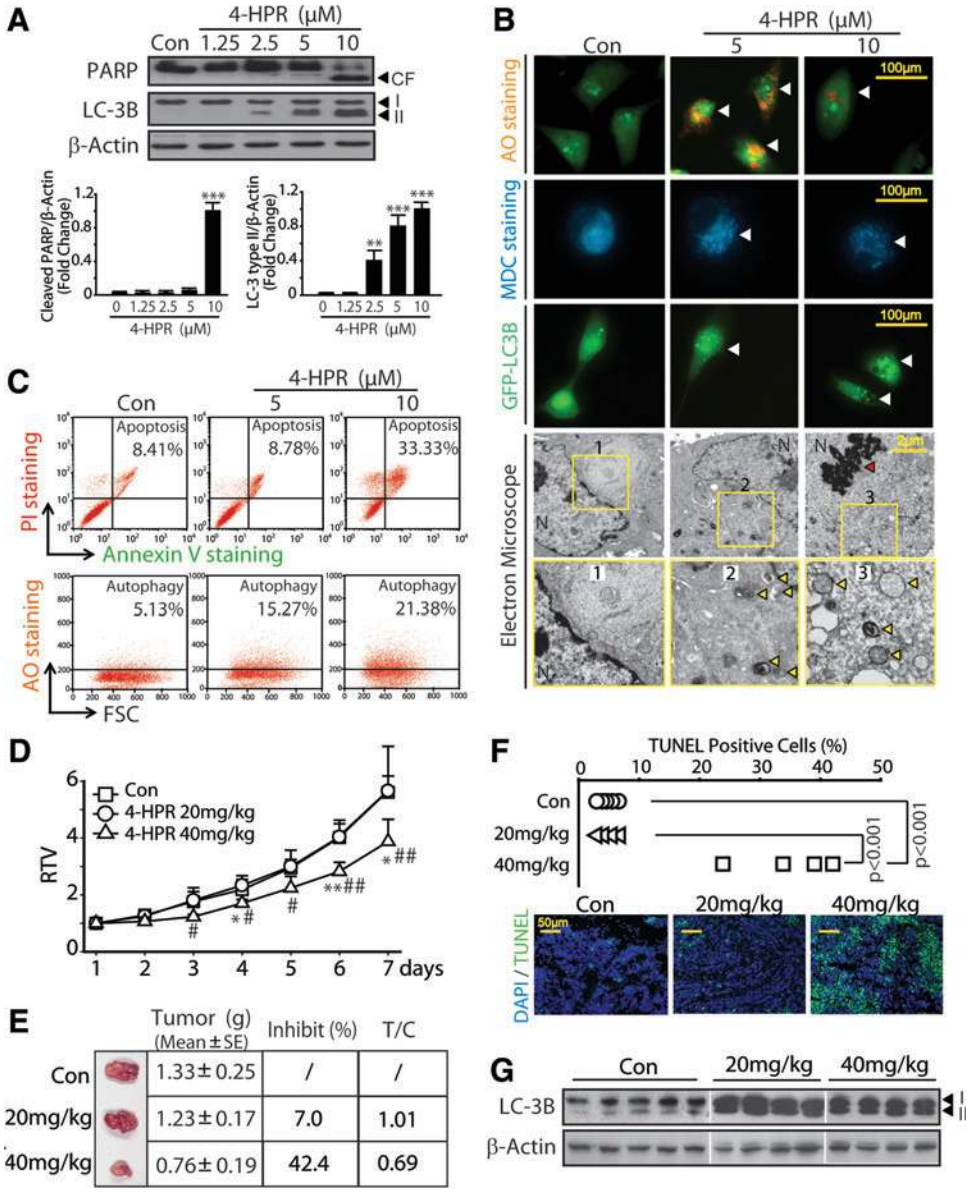

FIG. 1. 4-HPR pushes autophagy down to apoptosis in a concentration threshold-dependent manner *in vitro* and *in vivo*. **(A–C)** HeLa cells were treated with serial concentrations of 4-HPR for 24 h and evaluated to determine autophagy and apoptosis. **(A)** Total cell extracts were probed with antibodies against LC-3B, PARP, and β-Actin. The density of the immunoreactive bands was calculated by Quantity One software, and the data are shown as the ratio *versus* β-Actin. The data are expressed as the mean ± standard deviation (SD) ($n = 3$, $^{**}p < 0.01$, $^{***}p < 0.001$ *vs.* control). CF, cleaved fragment of PAPP; I, LC3-I; II, LC3-II. **(B)** Acridine orange (AO) staining, MDC staining, GFP-LC3 transfection assays, and electron microscopy were performed. *White arrow:* appearance of autophagosomes; *yellow arrow:* autophagosomes; *red arrow:* condensation of chromatin. **(C)** Fluorescence activated cell sorting (FACS) quantification of acidic vesicular organelles (AVOs) or apoptosis with acridine orange or annexin V/PI in HeLa cells exposed to 4-HPR. **(D–G)** The mice transplanted with human xenografts (HeLa) were randomly divided into three groups and given injections of serial doses of 4-HPR (20 or 40 mg/kg/day, i.v.) for a period of 7 days (n = at least 4). The tumor volume was recorded daily, and the relative tumor volume (RTV) was calculated. At the end of the experiment, the tumor was weighed and analyzed with TUNEL staining and western blotting. **(D)** RTV was expressed as the mean ± standard error (SE). $^{*}p < 0.05$, $^{**}p < 0.01$, 40 mg/kg *versus* control; $^{\#}p < 0.05$, $^{\#\#}p < 0.01$, 40 mg/kg *versus* 20 mg/kg. **(E)** Representative images of tumors in the different groups are shown along with the tumor weight (mean ± SE), inhibition rate, and T/C value (RTV of treatment/RTV of control). **(F)** The TUNEL-positive rate of each tumor was analyzed (*top panel*), and representative merged images of TUNEL staining of tumor tissues in the different groups (*bottom panel*) are shown. **(G)** Expression of LC-3B and β-Actin in tumor tissues from the different groups was detected by western blotting. To see this illustration in color, the reader is referred to the web version of this article at www.liebertpub.com/ars

epidermoid carcinoma KB cells (Supplementary Fig. S1A; Supplementary Data are available online at www.liebertpub.com/ars). Moreover, loss of the mitochondrial membrane potential ($\Delta\Psi m$), an indicator of mitochondrial injury, was only observed with 10 μM 4-HPR treatment in all 4 cancer cell lines (Supplementary Fig. S1B). Taken together, these results suggest that apoptosis can only be triggered by high concentrations of 4-HPR, whereas autophagy can be induced by very low concentrations of 4-HPR. Hence, these data not only indicate that increasing concentrations of 4-HPR push autophagy down to apoptosis but also suggest that the initiation of apoptosis is the key step of this process, as autophagy consistently occurs during 4-HPR treatment.

To further quantify autophagy and apoptosis, AO staining and annexin V-PI staining plus fluorescence activated cell sorting (FACS) analysis were used, respectively. As presented in Figure 1C, in the presence of AO, 4-HPR treatment (5 and 10 μM, 24 h) markedly increased the bright red fluorescence intensity (*y*-axis) from 5.13% to 15.27% and 21.38%; however, the number of annexin V^+ PI^+ cells [quadrant II, ''late apoptosis,'' or ''secondary necrotic'' (24)] was significantly increased only in the 10 μM 4-HPR group (from 8.41% to 33.33%) and not in the 5 μM 4-HPR group (from 8.41% to 8.78%). Once again, our results imply the existence of a potential concentration threshold for the effect of 4-HPR on pushing autophagy down to apoptosis.

To determine whether this process can be triggered by 4-HPR *in vivo*, we established an HeLa xenograft nude mouse model, which we treated with two doses of 4-HPR. As illustrated in Figure 1D and E, compared with the control group, the administration of 20 mg/kg 4-HPR resulted in weak or undetectable tumor weight inhibition (7.0% reduction), whereas treatment with 40 mg/kg 4-HPR significantly inhibited tumor growth by 42.4%. Similarly, the 40 mg/kg 4-HPR treatment had therapeutic activity, as indicated by a T/C value (RTV of treatment/RTV of control) of 0.69 (compared with 1.01 in the 20 mg/kg 4-HPR group). To ensure that the 4-HPR-mediated growth inhibition of HeLa xenografts was the result of cytotoxicity, we first detected apoptosis in HeLa xenografts by TUNEL staining. No TUNEL-positive cells were detected in the control and 20 mg/kg 4-HPR groups; however, a significant number of TUNEL-positive cells were found in the 40 mg/kg 4-HPR group (Fig. 1F). We next characterized the expression of LC3-II and observed that almost all of the xenograft-derived HeLa cells were LC3-II-positive after treatment with 20 or 40 mg/kg 4-HPR (Fig. 1G). Collectively, these data indicate that 4-HPR also induces a dose-threshold dependent effect on pushing autophagy down to apoptosis *in vivo*.

The effect of 4-HPR on pushing autophagy down to apoptosis is dependent on the levels of 4-HPR-driven ROS

Autophagy and apoptosis are generally considered antagonistic (10, 26). Moreover, we observed that 4-HPR-driven autophagy inhibited apoptosis, because pretreatment with 3-methyladenine (3-MA), an inhibitor of an early stage of autophagy (21), suppressed the production of LC3-II and the increase in PARP cleavage and apoptosis in HeLa cells that were treated with 4-HPR (Supplementary Fig. S1C, left panel); whereas the pan caspase inhibitor Z-VAD-FMK only affected late apoptosis induced by 10 μM 4-HPR (Supplementary Fig. S1C, right panel). We are, thus, encouraged to explore which molecules determine the effect of 4-HPR on pushing autophagy down to apoptosis. Our group and others previously reported that mitochondrial-derived ROS (such as superoxide and/or H_2O_2) mediate reversible 4-HPR cytotoxicity in cancer cells (1, 7, 31). Recent studies also revealed the critical roles of ROS in the regulation of autophagy (40). Therefore, we questioned whether ROS production contributes to 4-HPR-induced apoptosis and autophagy. As expected, significant ROS generation was observed after 1 h of exposure to 4-HPR (5 and 10 μM) compared with untreated cells (Fig. 2A). Importantly, the production of ROS in the 10 μM 4-HPR group was approximately twofold greater than that in the 5 μM 4-HPR group. Similar results were also observed using an oxidation-sensitive probe [Probe-1 (28), Supplementary Fig. S2A]. These data clearly indicate that different concentrations of 4-HPR caused variability in the intracellular oxidation status.

To further address the role of ROS in the effect of 4-HPR on pushing autophagy down to apoptosis, we pretreated HeLa cells with an ROS scavenger, N-acetyl-L-cysteine (NAC), followed by 4-HPR exposure for the next 24 h. Consistent with previous reports (7, 25), 2 mM NAC almost completely blocked autophagy caused by 5 μM 4-HPR and apoptosis triggered by 10 μM 4-HPR; however, 2 mM NAC could not inhibit autophagy caused by 10 μM 4-HPR. In contrast, 4 mM NAC could partially inhibit autophagy caused by 10 μM 4-HPR (Fig. 2B and Supplementary Fig. S2B). Similar results were also obtained using glutathione (GSH, Supplementary Fig. S2B, C), which is another ROS scavenger. In addition, NAC inhibited the 4-HPR-induced increase in the ROS levels in a dose-dependent manner (Fig. 2C). These data suggest the pivotal roles of ROS in 4-HPR-triggered autophagy and apoptosis.

The redox state of the cells could be affected by the balance between the production and clearance of ROS. Since GSH is the major antioxidant in cells against oxidative stress and a decrease of intracellular GSH has been observed during ischemia/reperfusion or chemical exposure (5, 8, 43), we examined the intracellular GSH levels after 4-HPR treatment. As shown in Figure 2D, although 4-HPR treatment decreases intracellular GSH levels, there was no apparent difference in GSH levels between 5 and 10 μM 4-HPR groups, suggesting that endogenous GSH is not the key factor for the effect of 4-HPR on pushing autophagy down to apoptosis. On the other hand, evidence has generally suggested that the oxidation of cysteine residues by ROS results in conformational, structural, and direct catalytic consequences in targeted signaling proteins (11). Our previous study also demonstrated that the cysteine residues of the Akt protein could be oxidized by 4-HPR-driven ROS (7). Therefore, in the current study, we examined the percentage of free sulfhydryl groups in intracellular proteins after administering 5 or 10 μM 4-HPR. As illustrated in Figure 2E, compared with the control group, the percentage of free sulfhydryl groups in intracellular proteins was effectively decreased in a time-dependent manner in both the 5 and 10 μM 4-HPR groups. Of note, 10 μM 4-HPR was better able to induce the oxidation of free sulfhydryl groups in intracellular proteins. Furthermore, pretreatment with 4 mM NAC rescued the decrease in intracellular GSH and free sulfhydryl groups in both 5 and 10 μM 4-HPR groups; whereas 2 mM NAC blocked these decreases only in the 5 μM 4-HPR group and inhibited them in the 10 μM 4-HPR group (Supplementary Fig. S2D). Taken together with the data in Figure 2, these results strongly suggest

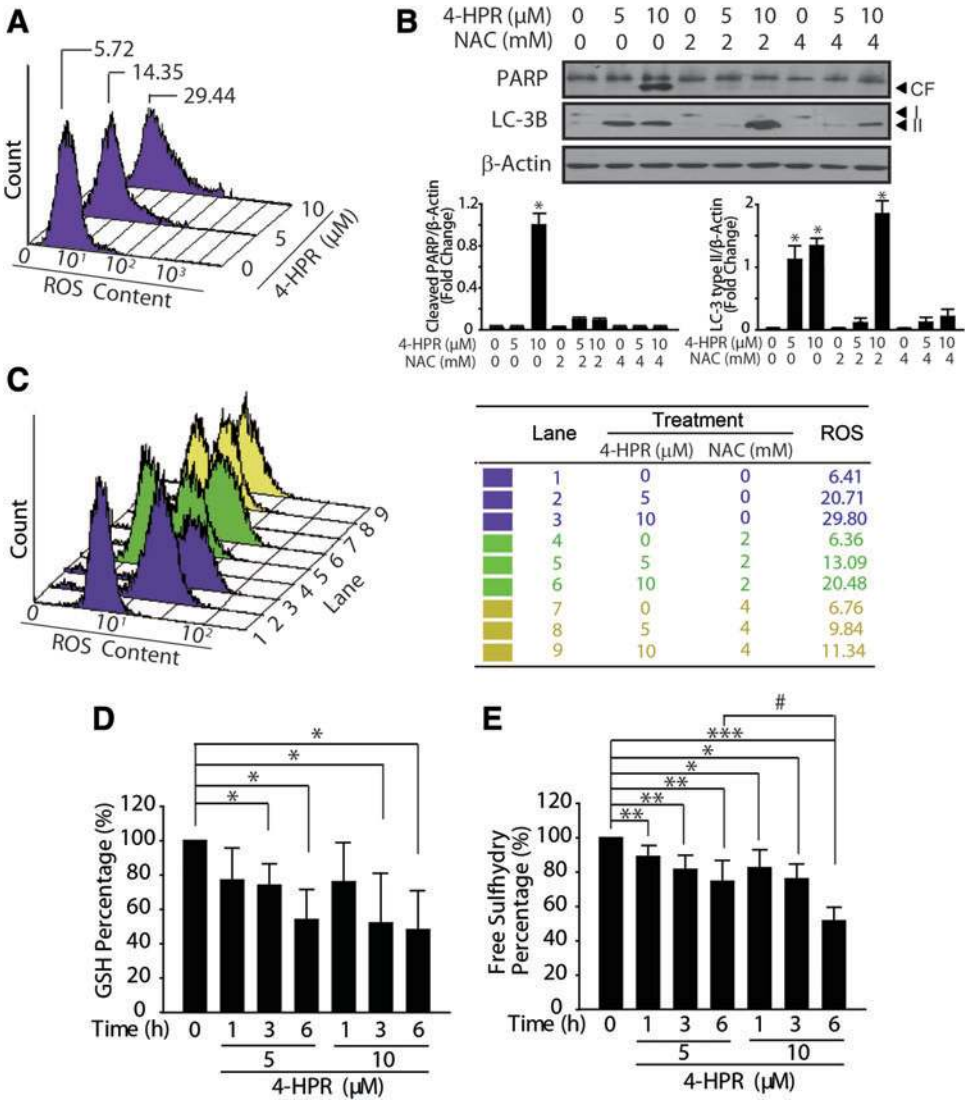

FIG. 2. The effect of 4-HPR on pushing autophagy down to apoptosis is dependent on the levels of 4-HPR-induced ROS. (A) HeLa cells were exposed to 5 or 10 μM 4-HPR for 1 h, and the mean level of ROS was determined using carboxy-DCFDA. **(B)** HeLa cells were pretreated with NAC (2 or 4 mM) for 0.5 h and exposed to 4-HPR for the next 24 h. Total cell extracts were probed with antibodies against LC-3B, PARP, and β-Actin. The density of immunoreactive bands was calculated by Quantity One software, and the data are shown as the ratio *versus* β-Actin. The data are expressed as the mean ± SD ($n = 3$, $^*p < 0.001$ *vs.* control). CF, cleaved fragment of PAPP; I, LC3-I; II, LC3-II. **(C)** HeLa cells were pretreated with NAC (2 or 4 mM) for 0.5 h and exposed to 4-HPR for the next 1 h. ROS levels were measured by FACS using carboxy-DCFDA. **(D, E)** Both the intracellular glutathione **(D)** and the percentage of free sulfhydryl groups in intracellular proteins **(E)** were determined after the cells were treated with 5 or 10 μM 4-HPR for the indicated time periods. Bars represent the mean ± SD of three independent experiments. *4-HPR treatment *versus* control ($^*p < 0.05$; $^{**}p < 0.01$; and $^{***}p < 0.001$); $^{\#}$10 μM 4-HPR *versus* 5 μM 4-HPR ($^{\#}p < 0.05$). NAC, N-acetyl-L-cysteine; ROS, reactive oxygen species. To see this illustration in color, the reader is referred to the web version of this article at www.liebertpub.com/ars

that the oxidation of free sulfhydryl groups, as regulated by ROS, may be the key factor involved in the effect of 4-HPR on pushing autophagy down to apoptosis.

ASK1-regulated JNK1 and p38 signaling pathways are responsible for 4-HPR-induced autophagy and apoptosis, respectively

ASK1-JNK/p38 is one of the most important signaling pathways involved in oxidative stress responses. Although JNKs and p38 are often grouped together as SAPKs and have similar physiological roles in many cases, it remains unclear whether activated JNKs and p38 play the same role in autophagy and apoptosis. MKK4, the co-upstream kinase of JNKs and p38, has no effect on the activation of autophagy, whereas the inhibition of MKK7 (the upstream kinase of JNKs) rescues autophagy (4, 42); thus, we hypothesize that JNKs and p38 may have diverse roles in the initiation of autophagy and apoptosis. Hence, we examined the phosphorylation status of these two proteins after 4-HPR treatment. As shown in Figure 3A, 10 μM 4-HPR induced sustained activation of JNK1 in HeLa cells; however, the activation of p38 was only observed in cells

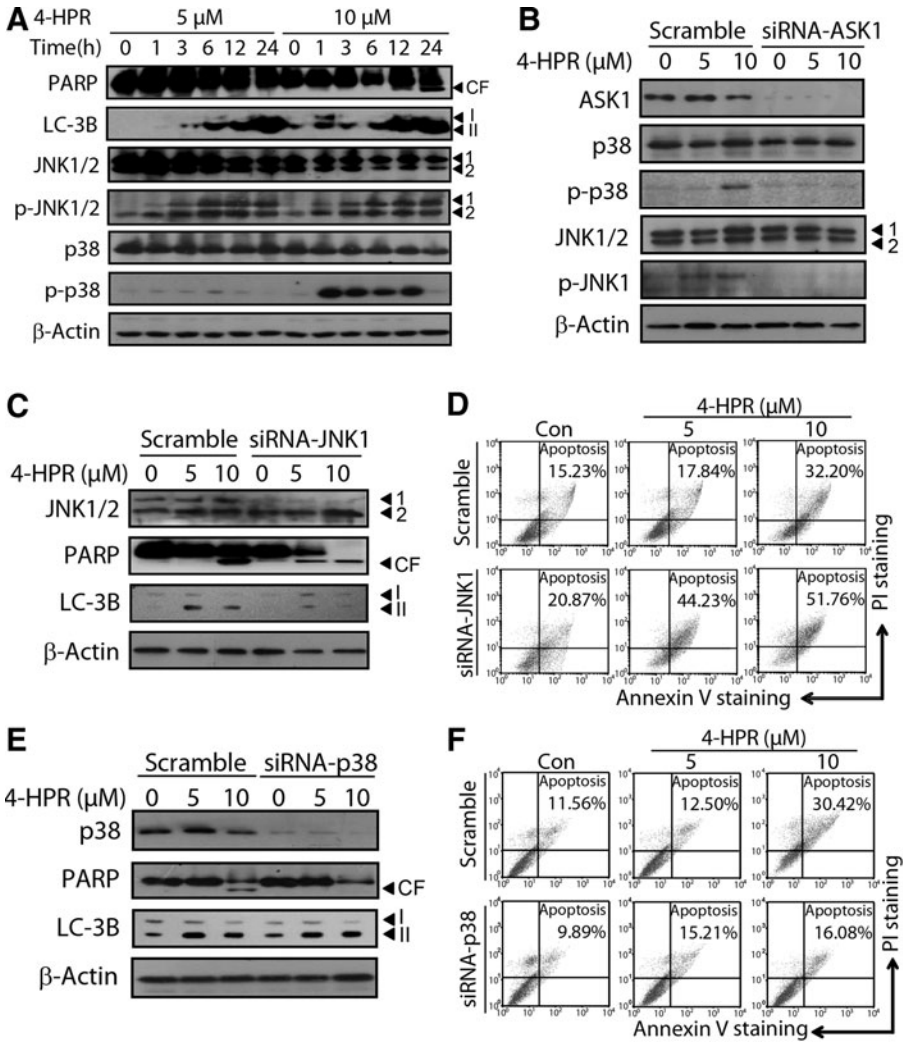

FIG. 3. ASK1-regulated JNK1 and p38 signaling pathways are responsible for 4-HPR-induced autophagy and apoptosis, respectively. (A) HeLa cells were treated with 5 or 10 μM 4-HPR for the indicated times, and the total cell extracts were probed with antibodies against LC-3B, PARP, JNK1/2, p-JNK1/2 (Thr183/Tyr185), p38, p-p38 (Thr180/Tyr182), and β-Actin. 1, JNK1 or p-JNK1; 2, JNK2 or p-JNK2; CF, cleaved fragment of PAPP; I, LC3-I; II, LC3-II. **(B)** ASK1 knockdown abolished the activation of JNK1 and p38 signaling induced by 4-HPR in HeLa cells. Cells were transfected with either 100 nM scrambled siRNA or 100 nM ASK1 siRNA for 24 h before exposure to 4-HPR for an additional 3 h. **(C–F)** HeLa cells transfected with siRNA against JNK1 or p38 were treated with 4-HPR for an additional 24 h and evaluated for autophagy and apoptosis. **(C, E)** Total cell extracts were probed with antibodies against JNK1, p38, LC-3B, PARP, and β-Actin. **(D, F)** Quantification of apoptosis in siRNA-transfected HeLa cells treated with 4-HPR using annexin V/PI followed by FACS analysis. All the immunoblots shown are from one representative experiment (out of three that gave similar results). β-Actin was used as the loading control. ASK1, apoptosis signal-regulating kinase 1; JNK, c-Jun N-terminal kinase; siRNA, small interfering RNA.

treated with 10 μM 4-HPR. Moreover, when we used a specific small interfering RNA (siRNA) targeted against ASK1, which is required for sustained activation of both JNK1 and p38 (17), the 4-HPR-triggered activation of JNK1 and p38 was greatly attenuated, as revealed by the reduction in phosphorylated protein accumulation in the ASK1 siRNA group compared with the scrambled siRNA group (Fig. 3B). This result suggests that ASK1-regulated JNK1 and p38 signaling pathways may be responsible for 4-HPR-induced autophagy and apoptosis, respectively.

To further validate this hypothesis, we utilized both siRNA and pharmacological inhibitors against JNK1 and p38. When JNK1 was silenced by a specific siRNA, the induction of LC3-II caused by 4-HPR (5 and 10 μM) was almost completely blocked, and an increase in late apoptosis was observed (Fig. 3C, D). Similarly, pretreatment with 20 μM SP600125 (a pharmacological inhibitor of JNK1) significantly blocked 4-HPR-driven autophagy but increased late apoptosis (Supplementary Fig. S3A, B). In contrast, when HeLa cells were pretreated with siRNA against p38 or with SB203580 (a pharmacological inhibitor of p38), late apoptosis was dramatically inhibited while autophagy was unaffected on 4-HPR treatment (Fig. 3E, F and Supplementary Fig. S3C, D). Collectively, these data further demonstrate that ASK1-activated JNK1 and p38 signaling are responsible for 4-HPR-induced autophagy and apoptosis, respectively. Along with

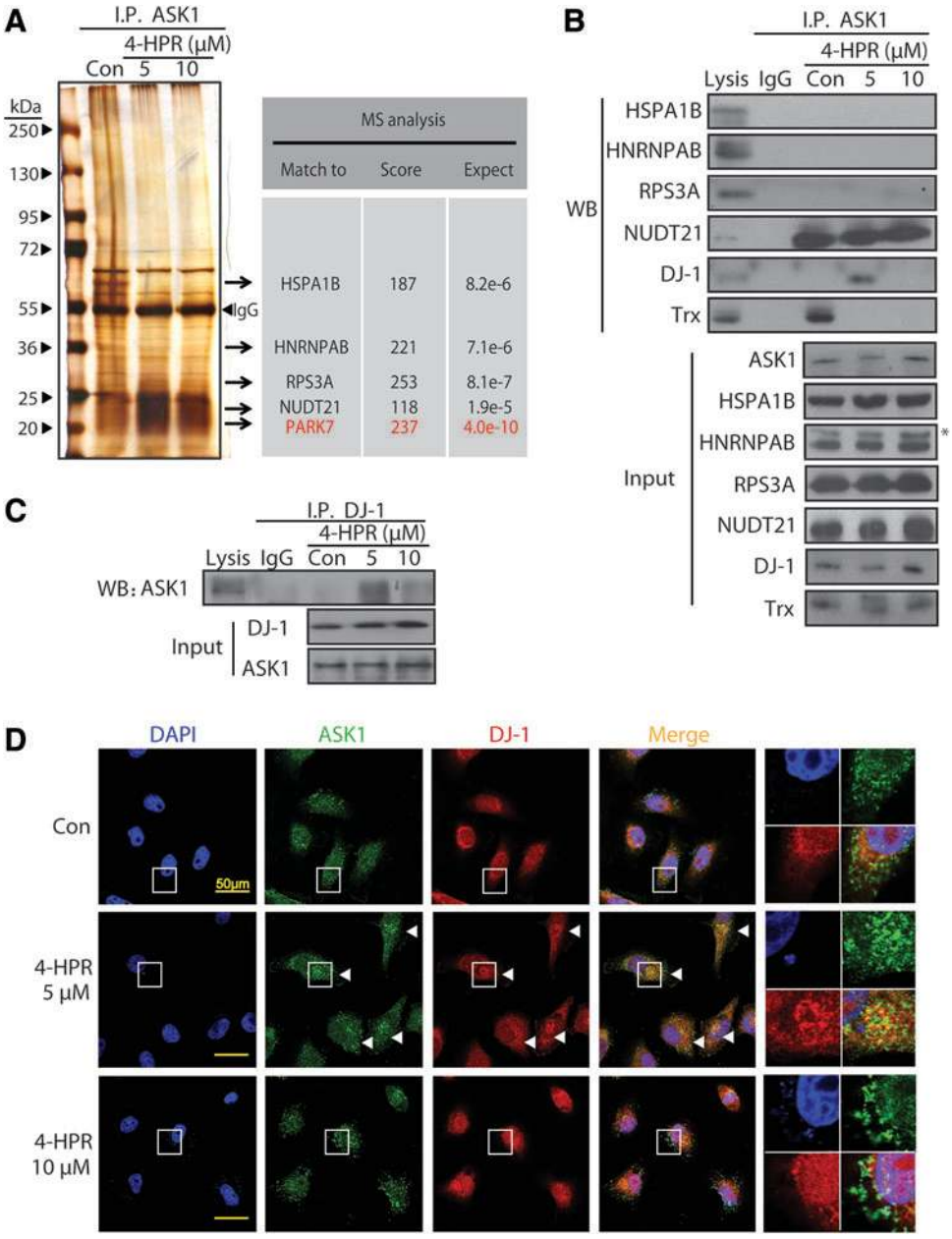

FIG. 4. ASK1 forms a complex with DJ-1 in the presence of mild levels of ROS but not in the presence of excessive levels of ROS. **(A, B)** HeLa cells were treated with 5 or 10 μM 4-HPR for 3 h followed by co-immunoprecipitation with anti-ASK1 antibody. **(A)** The immunoprecipitated proteins were separated by SDS-PAGE followed by silver staining (*left*), and LC-MS/MS analysis was conducted to identify proteins that differently bind to ASK1 under varied oxidative states. Five unique bands were identified, and their associated information is listed in the table (*right*). **(B)** An immunoprecipitation assay was performed to validate the interaction between DJ-1 and five unique proteins identified in the LC-MS/MS analysis. The cells were treated with 5 or 10 μM 4-HPR for 3 h, and co-immunoprecipitation was subsequently performed with an anti-ASK1 antibody. Trx was used as a positive control. Total cell extracts were also probed with antibodies against ASK1, HSPA1B, HNRNPAB, RPS3A, NUDT21, DJ-1, and Trx. *Nonspecific bands. **(C)** A reverse immunoprecipitation assay was performed to validate the interaction between DJ-1 and ASK1. HeLa cells were treated with 5 or 10 μM 4-HPR for 3 h, and co-immunoprecipitation was subsequently performed with an anti-DJ-1 antibody. The total cell extracts were also probed with antibodies against ASK1 or DJ-1. **(D)** Immunofluorescence analysis was performed to validate the interaction between DJ-1 and ASK1. HeLa cells treated with 5 or 10 μM 4-HPR for 3 h were probed with antibodies against DJ-1 (red) or ASK1 (green), and their immunofluorescence was analyzed. Enlarged views of each representative image (boxed) were shown on the right. *White arrows:* co-localization of ASK1 and DJ-1. LC-MS/MS, liquid chromatography-tandem mass spectrometry; Trx, thioredoxin. To see this illustration in color, the reader is referred to the web version of this article at www.liebertpub.com/ars

the results indicating that the initiation of apoptosis is the hallmark of the effect of 4-HPR on pushing autophagy down to apoptosis, our data also imply that the activation of p38 signaling is the critical step for such a process.

ASK1 forms a complex with DJ-1 under mild levels of ROS, but not under excessive levels of ROS

We next aimed at exploring how the cell finely regulates the activity of ASK1 and sequentially activates JNK1 or p38 signaling under low or high concentrations of 4-HPR. Since the regulatory mechanism of ASK1 activation has been revealed mainly through ASK1 binding proteins, we performed co-immunoprecipitation with an anti-ASK1 antibody followed by liquid chromatography-tandem mass spectrometry (LC-MS/MS) analysis to identify proteins that specifically bind to ASK1 under different oxidative states (Supplementary Fig. S4A). The results presented in Figure 4A demonstrate the separation of the ASK1 immunocomplex in HeLa cells treated with 5 or 10 μM 4-HPR by SDS-PAGE, with subsequent silver staining of the separated proteins. Of the more than 20 proteins visible by silver staining, five unique bands at $\sim$70, 40, 30, 25, and 20 kDa were identified and showed different trends among the three groups. These five bands were excised from the gel and subjected to in-gel tryptic digestion, and the resulting peptides were analyzed and identified by microspray LC-MS/MS techniques. The proteins in this study were identified automatically by computer software, and they are indicated in Figure. 4A and Supplementary Figure S4B. We further utilized an immunoprecipitation assay to validate these candidate proteins, and we found that only two proteins NUDT21 and PARK7 (also known as DJ-1) were pulled down with ASK1. In addition, the interaction between NUDT21 and ASK1 was nearly the same between the control and 4-HPR treatment groups, whereas DJ-1 (the mass spectrum of DJ-1 is illustrated in Supplementary Fig. S4C) interacted differently with ASK1 under the control *versus* 4-HPR treatment, similar to what was observed for Trx (Fig. 4B). Thus, our results suggest that DJ-1 may be conditionally associated with ASK1, which may be related to the different oxidative states triggered by 4-HPR treatment.

To validate the interaction between DJ-1 and ASK1 under different oxidative states, we performed a reciprocal immunoprecipitation assay. Only Trx can form a complex with ASK1 under basal conditions (Supplementary Fig. S4D); however, the immunoprecipitation of DJ-1 identified ASK1 only in HeLa cells treated with 5 μM 4-HPR (Fig. 4C). As expected, NAC pretreatment significantly modulated the interaction between DJ-1 and ASK1 (Supplementary Fig. S4E). Interestingly, the expression of DJ-1 and ASK1 was unchanged in HeLa cells that were treated with 5 or 10 μM 4-HPR, although the association between DJ-1 and ASK1 was remarkably increased in cells treated with 5 μM 4-HPR. This association disappeared in cells after exposure to 10 μM 4-HPR (Fig. 4B, C). Consistent with the immunoprecipitation results, the results of immunofluorescence analysis also confirmed direct co-localization of ASK1 (green) and DJ-1 (red) in the cytoplasm only under 5 μM 4-HPR treatment, as clearly demonstrated by merged immunofluorescence images (yellow signal, Fig. 4D). Given that (i) studies examining loss-of-function mutations have suggested that the antioxidant activity of DJ-1 results in its cytoprotective function in neuronal cells (38, 51); (ii) some clues of evidence have emerged that DJ-1 modulates p38 signaling through a physical interaction with ASK1 (33); (iii) our data demonstrate that the activation of p38 signaling induces apoptosis (Fig. 3); and (iv) our earlier data also indicate that DJ-1 is recruited to ASK1 under mild oxidative stress but segregates from ASK1 under lethal levels of oxidative stress (Fig. 4), we propose that DJ-1 may be a potent ''redox sensor'' which modulates the effect of 4-HPR on pushing autophagy down to apoptosis.

The oxidation states of DJ-1 mediate the activation of ASK1 by regulating DJ-1-ASK1 complex formation and dictate the cellular response to 4-HPR-induced ROS

The oxidative conversion of sulfhydryl groups at Cys residues to cysteine sulfinic acid (Cys-SO_2H) is likely to be responsible for DJ-1-mediated protection against oxidative stress. In addition, our data revealed that the oxidation of free sulfhydryl groups may be the key factor involved in the effect of 4-HPR on pushing autophagy down to apoptosis (Fig. 2E); thus, we examined the oxidative status of the DJ-1 protein under different levels of oxidative stress with the aim of understanding the critical role of DJ-1 as a sensor regulating 4-HPR's switch effect. An isoelectric focusing experiment revealed that DJ-1 had two different PI values in cells treated with 5 or 10 μM 4-HPR (Fig. 5A). Importantly, the PI value of DJ-1 isolated from cells treated with 10 μM 4-HPR was much lower than that of DJ-1 isolated from cells treated with 5 μM 4-HPR, indicating that this PI shift may be caused by an increase in intracellular oxidative stress triggered by 4-HPR. DJ-1 functions as a dimer (20, 51), and the oxidation of Cys46 and Cys53 may weaken the interactions at the dimer interface, leading to the formation of monomers (58). Therefore, we next examined the effect of different concentrations of 4-HPR on dimer formation *via* chemical cross-linking analysis using disuccinimidyl suberate (DSS), a primary amine-specific cross-linker that covalently cross-links proteins with their interactors. The results showed that in DSS-treated cell lysates, the levels of the dimeric form of DJ-1 were only decreased in the presence of 10 μM 4-HPR (Fig. 5B), indicating that only a high concentration of 4-HPR can affect the formation of DJ-1 dimers. Thus, different oxidative states of DJ-1 are involved in the effect of 4-HPR on pushing autophagy down to apoptosis: While ROS is tolerated, autophagy occurs and DJ-1 is mildly oxidized, whereas an excessive level of ROS causes apoptosis and further oxidation of DJ-1.

To determine the roles of the different oxidation states of DJ-1 in the effect of 4-HPR on pushing autophagy down to apoptosis, we further applied compound 23, which directly binds to DJ-1 and prevents excess oxidation (23), to assess whether the oxidation states of DJ-1 affect its ability to bind with ASK1 and activate downstream signaling. Consistent with the results in Figure 4B and C, DJ-1 dissociated from ASK1 under 10 μM 4-HPR treatment based on an immunoprecipitation assay; however, this dissociation was completely blocked by pretreatment with compound 23 (Fig. 5C), suggesting that only mildly oxidized DJ-1 can bind to ASK1, whereas highly oxidized DJ-1 dissociates from ASK1. Furthermore, pretreatment with compound 23 also blocked ASK1-activated p38 signaling under 10 μM 4-HPR treatment (Fig. 5D) and attenuated the apoptosis-

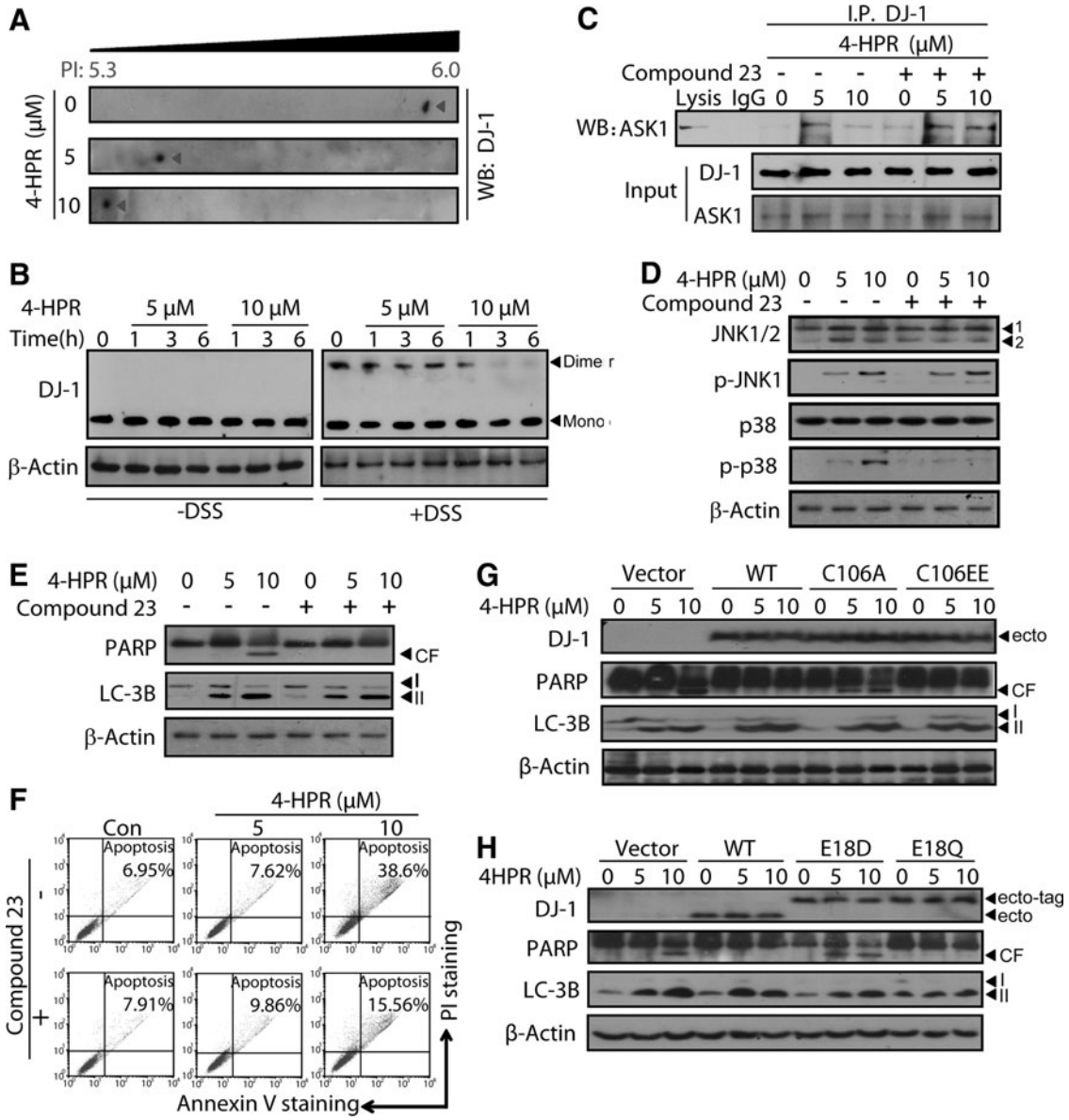

FIG. 5. The oxidation states of DJ-1 mediate the activation of ASK1 by regulating DJ-1-ASK1 complex formation and dictate the cellular response to 4-HPR-induced ROS. (A) HeLa cells were incubated with 5 or 10 μM 4-HPR for 3 h. The oxidation of DJ-1 was analyzed using isoelectric focusing electrophoresis followed by western blotting with an anti-DJ-1 antibody. **(B)** HeLa cells were incubated with 5 or 10 μM 4-HPR for the indicated times and subsequently treated with 0.5 mM DSS or DMSO for 2 h, and extracted proteins were analyzed by western blotting with an anti-DJ-1 antibody. **(C, D)** HeLa cells were pretreated with 10 μM compound 23 for 6 h, followed by 4-HPR exposure for an additional 3 h. Total cell extracts were analyzed by co-immunoprecipitation **(C)** or western blotting **(D)** with the indicated antibodies. **(E, F)** HeLa cells were pretreated with 10 μM compound 23 for 6 h, followed by 4-HPR exposure for an additional 3 h. The cells were then evaluated for autophagy and apoptosis. **(E)** Total cell extracts were probed with antibodies against LC-3B, PARP, and β-Actin. **(F)** Quantification of apoptosis with annexin V/PI plus FACS analysis. **(G, H)** HeLa cells were transfected with the indicated artificial DJ-1 mutants, followed by treatment with 5 or 10 μM 4-HPR for an additional 24 h. Total cell extracts were utilized to detect PARP cleavage and LC3-II accumulation. All the immunoblots shown are from one representative experiment (out of three that gave similar results). β-Actin was used as the loading control. 1, JNK1 or p-JNK1; 2, JNK2 or p-JNK2; CF, cleaved fragment of PAPP; I, LC3-I; II, LC3-II; DSS, disuccinimidyl suberate.

induction ability of 4-HPR without affecting autophagy (Fig. 5E, F), indicating that ASK1-DJ-1 binding is required for p38 activation and apoptosis induction. Taken together, these data are in agreement with the notion that the oxidation states of DJ-1 likely determine the cell fate by controlling ASK1 activation under 4-HPR treatment.

Previous reports have indicated that the cytoprotective activity of DJ-1 against oxidative stress is dependent on its cysteine residues (6, 45). Among the three cysteine residues of DJ-1, the most prominent is the easily oxidizable Cys106, which is in a constrained conformation (22, 52). In addition, it has been shown that the oxidation state of DJ-1 Cys106

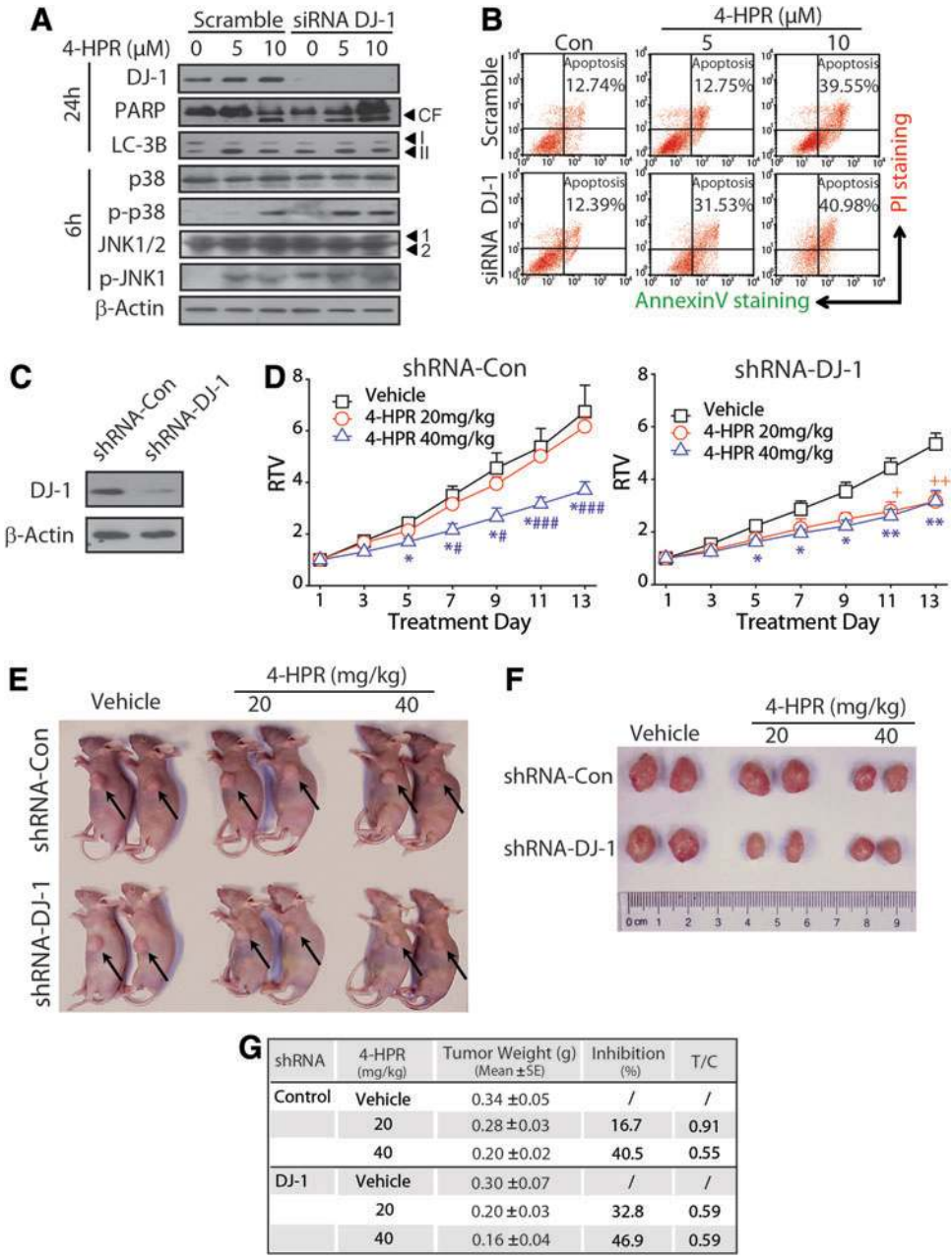

G

shRNA	4-HPR (mg/kg)	Tumor Weight (g) (Mean ±SE)	Inhibition (%)	T/C
Control	Vehicle	0.34 ±0.05	/	/
	20	0.28 ±0.03	16.7	0.91
	40	0.20 ±0.02	40.5	0.55
DJ-1	Vehicle	0.30 ±0.07	/	/
	20	0.20 ±0.03	32.8	0.59
	40	0.16 ±0.04	46.9	0.59

FIG. 6. DJ-1 depletion enhances the sensitivity of tumor cells to 4-HPR *in vitro* and *in vivo*. **(A, B)** DJ-1 knockdown enhanced the induction of apoptosis caused by 4-HPR (5 and 10 μM, 24 h). Cells were transfected with either 100 nM mock or DJ-1 siRNA for 24 h and subsequently exposed to 4-HPR treatment (5 and 10 μM, 6 or 24 h). The cells were analyzed by western blotting **(A)** or annexin V/PI staining plus FACS **(B)**. 1, JNK1 or p-JNK1; 2, JNK2 or p-JNK2; CF, cleaved fragment of PAPP; I, LC3-I; II, LC3-II. **(C–G)** DJ-1 depletion enhanced the sensitivity of tumor cells to 4-HPR *in vivo* in a xenograft nude mouse model generated using HeLa-shRNA-con or HeLa-shRNA-DJ-1 cells. **(C)** The HeLa cells were transduced with lentiviral pGFP-V-RS and pGFP-V-RS-DJ-1 as described in ''Methods'' section, and the knockdown efficiency was validated by western blotting. **(D–G)** The mice transplanted with HeLa-shRNA-con or HeLa-shRNA-DJ-1 xenografts were randomly divided into three groups and given injections of serial doses of 4-HPR (20 or 40 mg/kg/day, i.v.) for a period of 13 days ($n=6$). The tumor volume was recorded daily, and the RTV was calculated. **(D)** RTV was expressed as the mean ± SE. *40 mg/kg *versus* vehicle (*$p<0.05$; **$p<0.01$); $^{\#}$40 mg/kg *versus* 20 mg/kg ($^{\#}p<0.05$; $^{\#\#\#}p<0.001$). **(E, F)** Representative images of tumors (*black arrow*) in the different groups are shown. **(G)** At the end of the experiment, the tumors were weighed, and the inhibition rate and T/C value were calculated. To see this illustration in color, the reader is referred to the web version of this article at www.liebertpub.com/ars

regulates its interaction with ASK1 by incorporating an increasing number of oxygen atoms (50). Thus, we next generated two artificial DJ-1 mutants at position 106 by inserting two glutamate residues (referred to as C106EE) or by replacing cysteine with alanine (referred to as C106A). As shown in Figure 5G and Supplementary Figure S5A, transfection with wild type DJ-1 or C106EE DJ-1 conferred significant cytoprotection after 10 μM 4-HPR treatment when compared with vector controls. In contrast, the C106A mutant completely lost its cytoprotective activity as revealed by

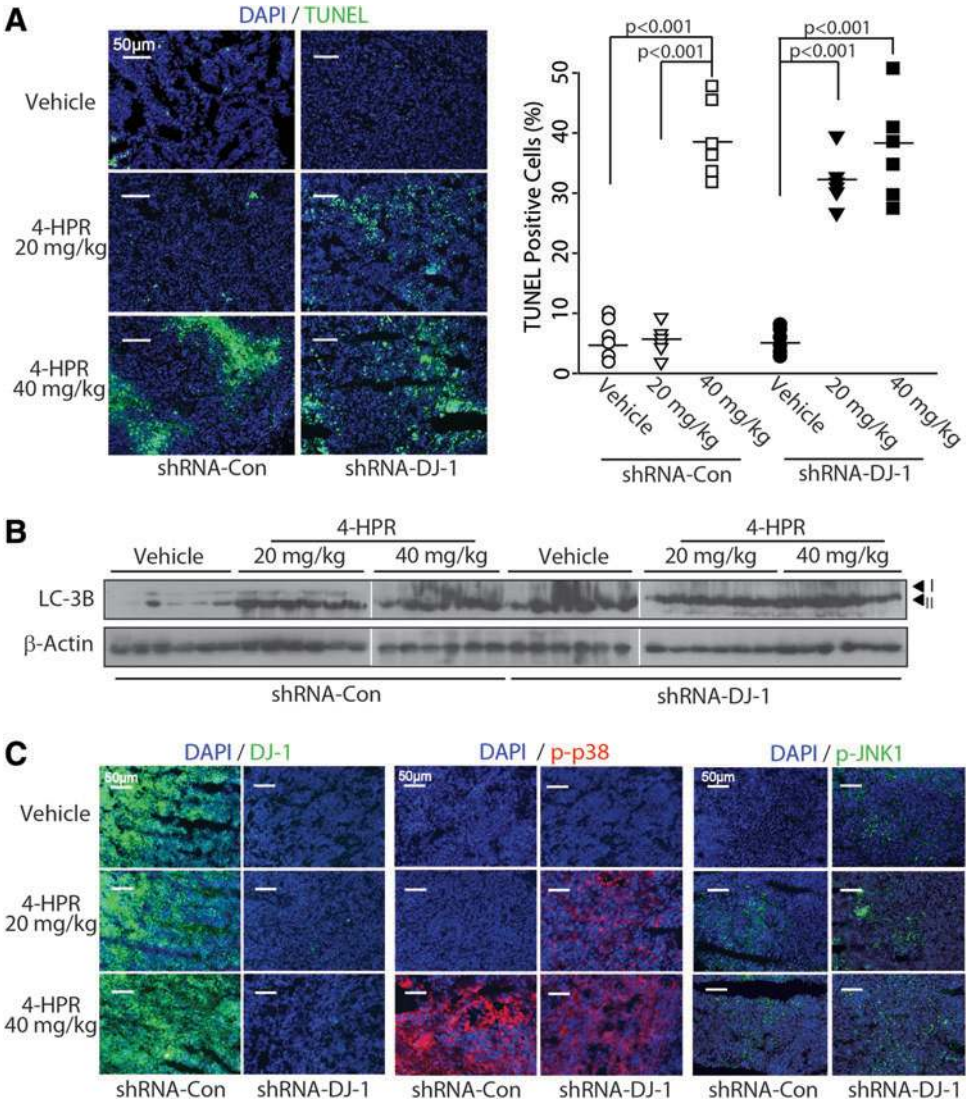

FIG. 7. DJ-1 depletion enhances the apoptosis-induction ability of 4-HPR by activating p38 signaling *in vivo*. **(A)** The TUNEL-positive rate of each tumor was analyzed (*right panel*), and representative merged images of TUNEL staining in the tumor tissues in different groups (*left panel*) are shown. **(B)** Expression of LC-3B and β-Actin in each tumor tissue from mice administered 4-HPR was detected by western blotting. I, LC3-I; II, LC3-II. **(C)** Tumors from each group were analyzed by immunofluorescence with antibodies against DJ-1 (green), p-p38 (red), or p-JNK1 (green). To see this illustration in color, the reader is referred to the web version of this article at www.liebertpub.com/ars

the appearance of a cleaved PARP fragment in cells treated with 5 or 10 μM 4-HPR. Of note, the autophagy-induction ability of 4-HPR was not altered in cells expressing either forms of DJ-1. Similar results were also observed in HeLa cells that were transfected with E18D DJ-1 or E18Q DJ-1 plasmids (Fig. 5H and Supplementary Fig. S5B), which are considered as regulating the oxidation state of DJ-1 Cys106 (2). Once again, our data demonstrate that while mild oxidation of DJ-1 is closely correlated with the cytoprotection process (for example, autophagy), extensive oxidized DJ-1 controls the initiation of apoptosis. Taken together, the current data support our hypothesis that DJ-1 may function as an intracellular redox sensor for the extent of ROS triggered by 4-HPR, and may determine the effect of 4-HPR on pushing autophagy down to apoptosis in tumor cells by controlling ASK1-p38 signaling.

DJ-1 depletion enhances the sensitivity of tumor cells to 4-HPR in vitro *and* in vivo

Finally, we sought to determine the biological significance of DJ-1 in 4-HPR-based chemotherapy. We observed that the *in vitro* anti-proliferation activity of 4-HPR (IC_{50} value) was negatively correlated with the protein expression level of DJ-1 in a panel of human cancer cell lines ($R = 0.815$) (Supplementary Fig. S5C), suggesting a correlation between the DJ-1 expression levels and sensitivity to 4-HPR chemotherapy. To further assess this finding, a specific siRNA targeted against DJ-1 (SiRNA-DJ-1) was preincubated with HeLa cells, which effectively blocked the expression of DJ-1 (Fig. 6A). Notably, DJ-1 depletion increased 4-HPR-driven late apoptosis to a greater extent in HeLa cells treated with 5 μM 4-HPR (from 15.75% to 33.53%) *versus* cells treated with 10 μM 4-HPR (from 42.55% to 47.98%) (Fig. 6B). A similar response was also observed for PARP cleavage and p38 activation but not for JNK activation. In contrast, the autophagy induced by 4-HPR was not affected by DJ-1 depletion, as revealed by the persistent accumulation of LC3-II in the SiRNA-DJ-1 group compared with the scrambled group (Fig. 6A). These data suggest that the silencing of DJ-1 enhances the sensitivity of HeLa cells to 4-HPR-driven apoptosis *in vivo*.

To test whether this enhancement effect could be reproduced *in vivo*, we evaluated the antitumor activity of 4-HPR in a xenograft nude mouse model generated with HeLa-shRNA-Con or HeLa-shRNA-DJ-1 cells (Fig. 6C). As illustrated in Figure 6D–G, in shRNA-Con xenografts, 40 mg/kg 4-HPR administration resulted in a moderate therapeutic effect, as the

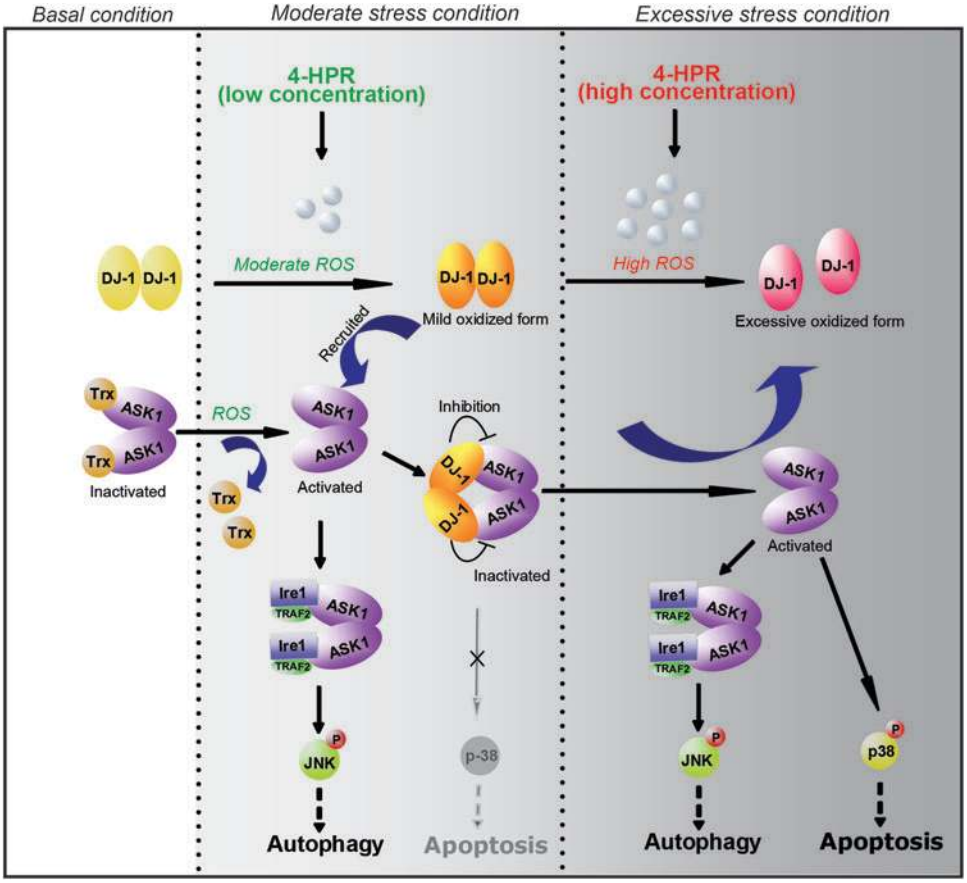

FIG. 8. Scheme for the effect of 4-HPR on pushing autophagy down to apoptosis. To see this illustration in color, the reader is referred to the web version of this article at www.liebertpub.com/ars

tumor volumes were significantly inhibited from days 5 to 13, the tumor weight was decreased by 40.5%, and the T/C value was only 0.55. Although 20 mg/kg 4-HPR weakly decreased tumor weight, it had no obvious effect on tumor volume or T/C value when compared with vehicle controls. Of note, although tumors derived from shRNA-DJ-1 cells grew 15%–20% slower than those derived from shRNA-Con cells (Fig. 6D), DJ-1 depletion significantly enhanced the sensitivity of shRNA-DJ-1 HeLa cells to 4-HPR, because the RTV, T/C value, and tumor weight decrease in the 20 mg/kg 4-HPR group were similar to those in the 40 mg/kg group. Thus, these data suggest that DJ-1 silencing enhances the sensitivity of HeLa cells to 4-HPR-induced growth arrest *in vivo*.

To ensure that DJ-1 silencing also enhances the sensitivity of HeLa cells to 4-HPR-induced apoptosis *in vivo*, we further detected apoptosis in the xenografts by TUNEL staining. Under 40 mg/kg treatment, the percentages of TUNEL-positive cells were similar between shRNA-Con and shRNA-DJ-1 groups; however, under 20 mg/kg treatment, more than 30% TUNEL-positive cells were observed in the shRNA-DJ-1 group, whereas there were almost no positive cells in the shRNA-Con group (Fig. 7A). In agreement with our *in vitro* data in Figure 6A and as previously reported (35), DJ-1 depletion increased the basal autophagy level and did not affect 4-HPR-caused autophagy (Fig. 7B). Furthermore, the results of immunofluorescence analysis also confirmed that DJ-1 depletion (Fig. 7C, left two panels) activated p38 in the 20 mg/kg 4-HPR group compared with the shRNA-Con group (Fig. 7C, middle two panels), whereas JNK1 remained inactivated (Fig. 7C, right two panels). Collectively, these data indicate that although the expansion of the DJ-1-depleted xenograft was decreased compared with that of the control group, DJ-1 depletion enhanced the sensitivity of tumor cells to 4-HPR-induced growth arrest and apoptosis both *in vitro* and *in vivo*.

Discussion

Chemotherapy-induced ROS not only contribute to apoptosis but also trigger autophagy in cancer cells. Since autophagy is reported to protect cancer cells from apoptosis, the therapeutic effect of chemotherapy is, thus, weakened. The identification of molecules that determine the cellular response to ROS is, therefore, important for the development of better strategies to increase chemotherapeutic efficiency. Here, we show that DJ-1 is one such regulator that senses the levels of ROS and determines the cellular response to 4-HPR by modifying its own oxidation status: Under mild oxidative stress, a moderately oxidized state of DJ-1 is recruited to ASK1 and inhibits its activity to keep the cell alive by activating autophagy; under a lethal level of oxidative stress, excessively oxidized DJ-1 is dissociated from ASK1, thereby activating it. Activated ASK1 then initiates the activation of p38 and enables the cells to commit apoptosis (Fig. 8).

It has been reported that DJ-1 is involved in the progression of early onset of familial Parkinson's disease, and recently, increasing reports have demonstrated its connection to cancer (16, 29, 48). The interaction between ASK1 and DJ-1 has been observed by several groups. For example, DJ-1 was found to interact directly with ASK1 and negatively

regulate its activation (33, 50). Further, DJ-1 has been shown to block the dissociation of Trx from ASK1, thereby retaining ASK1 in its inactive configuration (18). Of note, due to the connection between DJ-1 and Parkinson's disease, much of the work on their interaction has focused on the nervous system. Our present study confirms this interaction in a cancer model using the chemopreventive agent 4-HPR and reveals a new cellular function for DJ-1 as a redox sensor to determine cell fate on exposure to chemotherapeutics. We show that a moderately oxidized form of DJ-1, induced by treatment with 5 μm 4-HPR, will interact with ASK1 and inhibit its activity, whereas a highly oxidized form of DJ-1 will segregate from ASK1 and enable ASK1 to activate p38, thereby allowing apoptosis to occur. The ASK1-Trx complex has also been reported to function as a sensor of oxidative stress. It is not currently unknown whether Trx is involved in the ASK1-DJ-1 interaction in our model; however, Trx likely play an important role in the cellular response to 4-HPR-caused ROS. Trx forms a complex with ASK1 in the absence of oxidative stress and segregates from ASK1 once oxidative stress occurs, whereas DJ-1 is only recruited to ASK1 under oxidative stress conditions and can sense the degree of oxidative stress; therefore, it is possible that the Trx-ASK1 complex functions as the first redox gate by sensing the appearance of oxidative stress, while the DJ-1-ASK1 complex functions as the second redox gate by sensing the extent of oxidative stress. The relationship between these two redox sensors requires additional experimental scrutiny.

Both the crystal structure of DJ-1 and a substantial number of experiments have indicated that Cys106 might be an important residue for the function of DJ-1, and multi-oxidized forms of Cys106 have been observed (such as $-SO_2$ and $-SO_3$) (51). Although an increase in mitochondrial-derived ROS (such as superoxide and/or hydrogen peroxide) induced by 4-HPR has been observed in several tumor cells (1), it is still a challenge to identify which types of mitochondrial-derived ROS mediate the oxidation of DJ-1 on 4-HPR treatment. Interestingly, recent evidence suggests that the oxidation of Cys106 is usually caused by hydrogen peroxide both *in vitro* and *in vivo* (22). Unlike superoxide, hydrogen peroxide is membrane permeable. In addition, superoxide can either naturally dismute or be enzymatically dismuted (by MnSOD or Cu/ZnSOD) to hydrogen peroxide. Thus, it is highly likely that hydrogen peroxide plays a critical role in the 4-HPR-regulated oxidation of DJ-1. This hypothesis is partially supported by our preliminary results that hydrogen peroxide induces the effect of 4-HPR on pushing autophagy down to apoptosis in a concentration-dependent manner, similar to 4-HPR (Supplementary Fig. S2E). Further confirmation of the involvement of superoxide and hydrogen peroxide will be important in our future studies.

Although JNK and p38 signaling pathways are reported to have similar physiological roles in many cases, our data demonstrate that JNK1 and p38 have opposing functions in the initiation of autophagy and apoptosis, because JNK1 is responsible for autophagy and p38 is responsible for apoptosis induction. We found that DJ-1 inhibits or activates ASK1-p38 signaling in an oxidant dose-dependent manner, and although it remains unknown whether DJ-1 affects the activation of JNK1, our preliminary data regarding JNK1 activation might provide some clues. We examined the IRE1 and eIF2α signaling pathways, which are two branches of the unfolded protein response (35), and we found that IRE1 and eIF2α signaling mediate autophagy and apoptosis, respectively (Supplementary Fig. S6A, B). Considering that JNK1 activation mediated by ER stress requires ASK1-TRAF2-IRE1 complex formation (44), specific knockdown of IRE1 using siRNA was performed. As shown in Supplementary Figure S6C, the activation of endogenous JNK1 by 4-HPR (5 and 10 μM) was almost completely eliminated in the IRE1 siRNA group; whereas no change was observed in p38, suggesting that the ASK1-TRAF2-IRE1 complex is required for 4-HPR-induced activation of JNK1 but not for p38 activation. The formation of the ASK1-TRAF2-IRE1 complex in cells treated with 5 or 10 μM 4-HPR was also confirmed by an immunoprecipitation assay (Supplementary Fig. S6D). Our immunoprecipitation results demonstrate that both the DJ-1-ASK1 complex and the IRE1-TRAF2-ASK1 complex form in cells treated with 5 μM 4-HPR; however, they may form in a mutually exclusive manner, suggesting competition between these two protein complexes (Fig. 8). Although the affinity values of DJ-1-ASK1 and IRE1-TRAF2-ASK1 are poorly calculated, it has been demonstrated that both DJ-1 and TRAF2 can interact with the N-terminus of ASK1 (14, 50), which might explain our observations. Further studies are needed to investigate this phenomenon.

DJ-1 is currently viewed as a multifunctional protein with several proposed biochemical and cellular functions, including roles as a redox-regulated chaperone (41), cysteine protease (9, 34), RNA-binding protein (47), and transcriptional coactivator (53, 57). Although increasing reports have indicated its connection to cancer (16, 29, 48), DJ-1 has only been proposed as a biomarker for cancer diagnosis, prognosis, metastasis, or the sensitivity of chemotherapy. In the present study, we demonstrate that knocking down the expression of DJ-1 enhances the sensitivity of tumor cells to 4-HPR both *in vitro* and *in vivo* (Fig. 6). To our knowledge, we have provided the first *in vivo* evidence that DJ-1 depletion enhances the therapeutic benefit of chemoagents, supporting the idea that DJ-1 could be further recognized as a cancer therapeutic target. Considering the clinical limitations of siRNA or shRNA, the development of small molecular compounds targeting the cytoprotective function of DJ-1 might be an effective way to improve the outcome of chemotherapies. Given that both previous reports (51) and our data (Fig. 5C–H) demonstrate that Cys106 is an important residue required for the cytoprotective function of DJ-1, designing a small molecular compound that selectively binds to DJ-1 and oxidizes its Cys106 residue might be an effective strategy for inactivating DJ-1.

In summary, for the first time, we demonstrate the potential involvement of the ROS-mediated change in the DJ-1 oxidation state in the effect of 4-HPR on pushing autophagy down to apoptosis. This change mediates the activation of ASK1 by regulating DJ-1-ASK1 complex formation. These observations enhance our understanding of the mechanisms involved in the switch from autophagy to apoptosis triggered by anticancer drug-driven ROS and provide direct evidence to support the use of DJ-1 as a cancer therapeutic target.

Materials and Methods

Reagents, plasmids, and cell lines

4-HPR was kindly provided by Dr. B.J. Maurer (Children's Hospital, Los Angeles, CA). Compound-23 was purchased from Enamine Ltd. (Kiev, Ukraine), and SP600125 and

SB203580 were purchased from Calbiochem, Merck (San Diego, CA). Other reagents were purchased from Sigma-Aldrich (St. Louis, MO). All chemicals were dissolved in DMSO and stored in aliquots at −20°C.

The full-length DJ-1 coding sequence was amplified from the HeLa cDNA library using a pair of primers (Forward: GAGGCGATCGATGGCTTCCAAAAGAGC; Reverse: GCG ACGCGTCTAGTCTTTAAGAACAAGTGGAG) containing the SgfI or *Mlu*I restriction site and, subsequently, subcloned into the PCMV6 plasmid (Origene, Rockville, MD) to construct the tag-free or myc-tag plasmid. The indicated DJ-1 mutations were produced by site-directed mutagenesis (Transgene, Beijing, China) following the manufacturer's protocol.

HeLa, MG-63, HepG2, KB, and HCT116 cell lines were purchased from the Cell Bank of Type Culture Collection of Chinese Academy of Sciences (Shanghai, China) and were cultured in DMEM (Invitrogen, Carlsbad, CA), supplemented with 10% fetal bovine serum in a humidified atmosphere of 5% CO_2 at 37°C.

siRNA and plasmid transfection

siRNA duplexes targeted against human DJ-1, JNK1, p38, ASK-1, and CHOP as well as control scrambled siRNA were synthesized by Shanghai GenePharma Co., Ltd. The sense strands of the siRNAs against DJ-1, JNK1, p38, and ASK-1 were as follows: DJ-1: UGGAGACGGUCAUCCCUGUTT, JNK1: GGACUUACGUUGAAAACAGTT, p38: CUGCGG UUACUUAAACAUATT, ASK-1: GGUAUACAUGAGU GGAAUUTT, CHOP: GAGCUCUGAUUGACCGAAUGG UGAA. The siRNA against human IRE-1 was purchased from Thermo Scientific, Inc. (Bremen, Germany).

The siRNA and plasmid transfection were performed as previously described (30).

Lentivirus transduction

The lentiviral shRNA vector pGFP-V-RS was obtained from Origene (Rockville, MD), and the construct targeting DJ-1 was designed according to siRNA-DJ-1 (mentioned earlier) and constructed by the Genescript company (Nanjing, China). Virions were prepared at 48 h after transfection of 293FT cells, and virion titers were determined as described. HeLa cells were transduced with lentiviral pGFP-V-RS and pGFP-V-RS-DJ-1, as previously described (55).

RT-PCR, Western blotting, and immunoprecipitation

RT-PCR, Western blotting, and immunoprecipitation were performed as previously described (56).

Detection of intracellular ROS, GSH, and free sulfhydryl group in proteins

Detection of intracellular ROS was performed as previously described (7). The GSH assay was carried out following the manufacturer's suggested protocol (Jiancheng, Nanjing, China). Detection of free sulfhydryl group on proteins was performed based on the Ellman assay and is described in the Supplementary Data.

Isoelectric focusing

HeLa cells were incubated with 4-HPR for 3 h, and total protein extracted from the cells was separated in the pH range of 5.3–6.0 by isoelectric focusing gel electrophoresis. The proteins were then transferred to PVDF membranes, which were blotted with an anti-DJ-1 antibody.

Immunofluorescence and TUNEL staining

Immunofluorescence analysis was performed as previously described (7). TUNEL staining was performed following the manufacturer's protocol (Invitrogen, Grand Island, NY).

Cell proliferation assay and flow cytometric analysis for autophagy and apoptosis

Cell proliferation and flow cytometric analyses to determine apoptosis were performed as previously described (7, 30).

The treated cells were incubated with 1 μg/ml acridine orange for 15 min at 37°C. For quantification, green (510–530 nm) and red (650 nm) fluorescence emission from 10^4 cells was measured with an FACS-Calibur (BD Biosciences, Heidelberg, Germany).

Silver staining and LC-MS/MS analysis

Immunoprecipitated proteins were separated by SDS-PAGE followed by silver staining (44) and LC-MS/MS analysis (for details, see Supplementary Data).

Measurement of in vivo *activity*

Tumors were established by an injection of shRNA-transfected HeLa cells (5×10^6 cells/animal, subcutaneously into the armpit of the athymic mice) into 4- to 5-week-old BALB/c female athymic mice (National Rodent Laboratory Animal Resource, Shanghai, China). Treatments were initiated when the tumors reached a mean group size of $\sim$100–200 mm^3. Tumor volume (mm^3) was measured with calipers, and calculated as $(W^2\times L)/2$, where W is the width and L is the length. The T/C% was determined by calculating relative tumor volume (RTV) as T/C% = 100 × (mean RTV of treated group)/(mean RTV of control group). The tumor growth inhibition rate was calculated by using the following formula: inhibition rate (%) = (1 − TWt/TWc) × 100, where TWt and TWc are the mean tumor weight of the treatment and control groups, respectively. Athymic mice were intravenously administered with 4-HPR (20 and 40 mg/kg) that was dissolved in ethanol/cremophor EL/0.9% sterile sodium chloride solution (1:1:8, vol) once daily. Mouse weight and tumor volume were recorded daily until the animals were sacrificed. The animal study was approved by the Animal Research Committee at Zhejiang University (log number Zju2011101065 and Zju2012101016), and animal care was provided in accordance with institutional guidelines.

Statistical analysis

For all parameters measured, the values for all samples in the different experimental conditions were averaged, and the standard error or standard deviation of the mean was calculated. Analysis of variance followed by Student's *t*-test was used for the statistical analyses. Significance was defined as $p<0.05$.

Acknowledgment

This work was supported by grants from the National Natural Science Foundation of China No. 81273535 and No. 81202558.

Author Disclosure Statement

There is no conflict of interest to declare.

References

1. Asumendi A, Morales MC, Alvarez A, Arechaga J, and Perez-Yarza G. Implication of mitochondria-derived ROS and cardiolipin peroxidation in N-(4-hydroxyphenyl)retinamide-induced apoptosis. *Br J Cancer* 86: 1951–1956, 2002.
2. Blackinton J, Lakshminarasimhan M, Thomas KJ, Ahmad R, Greggio E, Raza AS, Cookson MR, and Wilson MA. Formation of a stabilized cysteine sulfinic acid is critical for the mitochondrial function of the parkinsonism protein DJ-1. *J Biol Chem* 284: 6476–6485, 2009.
3. Boulares AH, Yakovlev AG, Ivanova V, Stoica BA, Wang G, Iyer S, and Smulson M. Role of poly(ADP-ribose) polymerase (PARP) cleavage in apoptosis. Caspase 3-resistant PARP mutant increases rates of apoptosis in transfected cells. *J Biol Chem* 274: 22932–22940, 1999.
4. Byun JY, Yoon CH, An S, Park IC, Kang CM, Kim MJ, and Lee SJ. The Rac1/MKK7/JNK pathway signals upregulation of Atg5 and subsequent autophagic cell death in response to oncogenic Ras. *Carcinogenesis* 30: 1880–1888, 2009.
5. Cai YJ, Lu JJ, Zhu H, Xie H, Huang M, Lin LP, Zhang XW, and Ding J. Salvicine triggers DNA double-strand breaks and apoptosis by GSH-depletion-driven H2O2 generation and topoisomerase II inhibition. *Free Radic Biol Med* 45: 627–635, 2008.
6. Canet-Aviles RM, Wilson MA, Miller DW, Ahmad R, McLendon C, Bandyopadhyay S, Baptista MJ, Ringe D, Petsko GA, and Cookson MR. The Parkinson's disease protein DJ-1 is neuroprotective due to cysteine-sulfinic acid-driven mitochondrial localization. *Proc Natl Acad Sci U S A* 101: 9103–9108, 2004.
7. Cao J, Xu D, Wang D, Wu R, Zhang L, Zhu H, He Q, and Yang B. ROS-driven Akt dephosphorylation at Ser-473 is involved in 4-HPR-mediated apoptosis in NB4 cells. *Free Radic Biol Med* 47: 536–547, 2009.
8. Casini AF, Pompella A, and Comporti M. Liver glutathione depletion induced by bromobenzene, iodobenzene, and diethylmaleate poisoning and its relation to lipid peroxidation and necrosis. *Am J Pathol* 118: 225–237, 1985.
9. Chen J, Li L, and Chin LS. Parkinson disease protein DJ-1 converts from a zymogen to a protease by carboxyl-terminal cleavage. *Hum Mol Genet* 19: 2395–2408, 2010.
10. Cook KL, Shajahan AN, Warri A, Jin L, Hilakivi-Clarke LA, and Clarke R. Glucose-regulated protein 78 controls cross-talk between apoptosis and autophagy to determine antiestrogen responsiveness. *Cancer Res* 72: 3337–3349, 2012.
11. Cross JV and Templeton DJ. Regulation of signal transduction through protein cysteine oxidation. *Antioxid Redox Signal* 8: 1819–1827, 2006.
12. Cuperus R, Leen R, Tytgat GA, Caron HN, and van Kuilenburg AB. Fenretinide induces mitochondrial ROS and inhibits the mitochondrial respiratory chain in neuroblastoma. *Cell Mol Life Sci* 67: 807–816, 2009.
13. Fazi B, Bursch W, Fimia GM, Nardacci R, Piacentini M, Di Sano F, and Piredda L. Fenretinide induces autophagic cell death in caspase-defective breast cancer cells. *Autophagy* 4: 435–441, 2008.
14. Fujino G, Noguchi T, Matsuzawa A, Yamauchi S, Saitoh M, Takeda K, and Ichijo H. Thioredoxin and TRAF family proteins regulate reactive oxygen species-dependent activation of ASK1 through reciprocal modulation of the N-terminal homophilic interaction of ASK1. *Mol Cell Biol* 27: 8152–8163, 2007.
15. Gupta SC, Hevia D, Patchva S, Park B, Koh W, and Aggarwal BB. Upsides and downsides of reactive oxygen species for cancer: the roles of reactive oxygen species in tumorigenesis, prevention, and therapy. *Antioxid Redox Signal* 16: 1295–1322, 2011.
16. He X, Zheng Z, Li J, Ben Q, Liu J, Zhang J, Ji J, Yu B, Chen X, Su L, Zhou L, Liu B, and Yuan Y. DJ-1 promotes invasion and metastasis of pancreatic cancer cells by activating SRC/ERK/uPA. *Carcinogenesis* 33: 555–562, 2012.
17. Ichijo H, Nishida E, Irie K, ten Dijke P, Saitoh M, Moriguchi T, Takagi M, Matsumoto K, Miyazono K, and Gotoh Y. Induction of apoptosis by ASK1, a mammalian MAPKKK that activates SAPK/JNK and p38 signaling pathways. *Science* 275: 90–94, 1997.
18. Junn E, Taniguchi H, Jeong BS, Zhao X, Ichijo H, and Mouradian MM. Interaction of DJ-1 with Daxx inhibits apoptosis signal-regulating kinase 1 activity and cell death. *Proc Natl Acad Sci U S A* 102: 9691–9696, 2005.
19. Kabeya Y, Mizushima N, Ueno T, Yamamoto A, Kirisako T, Noda T, Kominami E, Ohsumi Y, and Yoshimori T. LC3, a mammalian homologue of yeast Apg8p, is localized in autophagosome membranes after processing. *EMBO J* 19: 5720–5728, 2000.
20. Kahle PJ, Waak J, and Gasser T. DJ-1 and prevention of oxidative stress in Parkinson's disease and other age-related disorders. *Free Radic Biol Med* 47: 1354–1361, 2009.
21. Kim J and Klionsky DJ. Autophagy, cytoplasm-to-vacuole targeting pathway, and pexophagy in yeast and mammalian cells. *Annu Rev Biochem* 69: 303–342, 2000.
22. Kinumi T, Kimata J, Taira T, Ariga H, and Niki E. Cysteine-106 of DJ-1 is the most sensitive cysteine residue to hydrogen peroxide-mediated oxidation *in vivo* in human umbilical vein endothelial cells. *Biochem Biophys Res Commun* 317: 722–728, 2004.
23. Kitamura Y, Watanabe S, Taguchi M, Takagi K, Kawata T, Takahashi-Niki K, Yasui H, Maita H, Iguchi-Ariga SM, and Ariga H. Neuroprotective effect of a new DJ-1-binding compound against neurodegeneration in Parkinson's disease and stroke model rats. *Mol Neurodegener* 6: 48, 2011.
24. Krysko DV, D'Herde K, and Vandenabeele P. Clearance of apoptotic and necrotic cells and its immunological consequences. *Apoptosis* 11: 1709–1726, 2006.
25. Lai WL and Wong NS. The PERK/eIF2 alpha signaling pathway of Unfolded Protein Response is essential for N-(4-hydroxyphenyl)retinamide (4HPR)-induced cytotoxicity in cancer cells. *Exp Cell Res* 314: 1667–1682, 2008.
26. Lepine S, Allegood JC, Edmonds Y, Milstien S, and Spiegel S. Autophagy induced by deficiency of sphingosine-1-phosphate phosphohydrolase 1 is switched to apoptosis by calpain-mediated autophagy-related gene 5 (Atg5) cleavage. *J Biol Chem* 286: 44380–44390, 2011.
27. Li X, Ling W, Pennisi A, Khan S, and Yaccoby S. Fenretinide inhibits myeloma cell growth, osteoclastogenesis and osteoclast viability. *Cancer Lett* 284: 175–181, 2009.
28. Li X, Qian S, He Q, Yang B, Li J, and Hu Y. Design and synthesis of a highly selective fluorescent turn-on probe for thiol bioimaging in living cells. *Org Biomol Chem* 8: 3627–3630, 2010.

29. Liu S, Yang Z, Wei H, Shen W, Liu J, Yin Q, Li X, and Yi J. Increased DJ-1 and its prognostic significance in hepatocellular carcinoma. *Hepatogastroenterology* 57: 1247–1256, 2011.
30. Liu XW, Su Y, Zhu H, Cao J, Ding WJ, Zhao YC, He QJ, and Yang B. HIF-1alpha-dependent autophagy protects HeLa cells from fenretinide (4-HPR)-induced apoptosis in hypoxia. *Pharmacol Res* 62: 416–425, 2010.
31. Maurer BJ, Metelitsa LS, Seeger RC, Cabot MC, and Reynolds CP. Increase of ceramide and induction of mixed apoptosis/necrosis by N-(4-hydroxyphenyl)- retinamide in neuroblastoma cell lines. *J Natl Cancer Inst* 91: 1138–1146, 1999.
32. Mizushima N and Yoshimori T. How to interpret LC3 immunoblotting. *Autophagy* 3: 542–545, 2007.
33. Mo JS, Jung J, Yoon JH, Hong JA, Kim MY, Ann EJ, Seo MS, Choi YH, and Park HS. DJ-1 modulates the p38 mitogen-activated protein kinase pathway through physical interaction with apoptosis signal-regulating kinase 1. *J Cell Biochem* 110: 229–237, 2010.
34. Olzmann JA, Brown K, Wilkinson KD, Rees HD, Huai Q, Ke H, Levey AI, Li L, and Chin LS. Familial Parkinson's disease-associated L166P mutation disrupts DJ-1 protein folding and function. *J Biol Chem* 279: 8506–8515, 2004.
35. Ren H, Fu K, Mu C, Li B, Wang D, and Wang G. DJ-1, a cancer and Parkinson's disease associated protein, regulates autophagy through JNK pathway in cancer cells. *Cancer Lett* 297: 101–108, 2010.
36. Runchel C, Matsuzawa A, and Ichijo H. Mitogen-activated protein kinases in mammalian oxidative stress responses. *Antioxid Redox Signal* 15: 205–218, 2010.
37. Sabichi AL, Lerner SP, Atkinson EN, Grossman HB, Caraway NP, Dinney CP, Penson DF, Matin S, Kamat A, Pisters LL, Lin DW, Katz RL, Brenner DE, Hemstreet GP, 3rd, Wargo M, Bleyer A, Sanders WH, Clifford JL, Parnes HL, and Lippman SM. Phase III prevention trial of fenretinide in patients with resected non-muscle-invasive bladder cancer. *Clin Cancer Res* 14: 224–229, 2008.
38. Saeed U, Ray A, Valli RK, Kumar AM, and Ravindranath V. DJ-1 loss by glutaredoxin but not glutathione depletion triggers Daxx translocation and cell death. *Antioxid Redox Signal* 13: 127–144, 2009.
39. Saitoh M, Nishitoh H, Fujii M, Takeda K, Tobiume K, Sawada Y, Kawabata M, Miyazono K, and Ichijo H. Mammalian thioredoxin is a direct inhibitor of apoptosis signal-regulating kinase (ASK) 1. *EMBO J* 17: 2596–2606, 1998.
40. Scherz-Shouval R and Elazar Z. ROS, mitochondria and the regulation of autophagy. *Trends Cell Biol* 17: 422–427, 2007.
41. Shendelman S, Jonason A, Martinat C, Leete T, and Abeliovich A. DJ-1 is a redox-dependent molecular chaperone that inhibits alpha-synuclein aggregate formation. *PLoS Biol* 2: e362, 2004.
42. Shimizu S, Konishi A, Nishida Y, Mizuta T, Nishina H, Yamamoto A, and Tsujimoto Y. Involvement of JNK in the regulation of autophagic cell death. *Oncogene* 29: 2070–2082, 2010.
43. Stanislawski L, Lefeuvre M, Bourd K, Soheili-Majd E, Goldberg M, and Perianin A. TEGDMA-induced toxicity in human fibroblasts is associated with early and drastic glutathione depletion with subsequent production of oxygen reactive species. *J Biomed Mater Res A* 66: 476–482, 2003.
44. Stochaj WR, Berkelman T, and Laird N. Mass spectrometry-compatible silver staining. *CSH Protoc* 2007: pdb.prot4742, 2007.
45. Taira T, Saito Y, Niki T, Iguchi-Ariga SM, Takahashi K, and Ariga H. DJ-1 has a role in antioxidative stress to prevent cell death. *EMBO Rep* 5: 213–218, 2004.
46. Tiwari M, Bajpai VK, Sahasrabuddhe AA, Kumar A, Sinha RA, Behari S, and Godbole MM. Inhibition of N-(4-hydroxyphenyl)retinamide-induced autophagy at a lower dose enhances cell death in malignant glioma cells. *Carcinogenesis* 29: 600–609, 2008.
47. van der Brug MP, Blackinton J, Chandran J, Hao LY, Lal A, Mazan-Mamczarz K, Martindale J, Xie C, Ahmad R, Thomas KJ, Beilina A, Gibbs JR, Ding J, Myers AJ, Zhan M, Cai H, Bonini NM, Gorospe M, and Cookson MR. RNA binding activity of the recessive parkinsonism protein DJ-1 supports involvement in multiple cellular pathways. *Proc Natl Acad Sci U S A* 105: 10244–10249, 2008.
48. Vasseur S, Afzal S, Tomasini R, Guillaumond F, Tardivel-Lacombe J, Mak TW, and Iovanna JL. Consequences of DJ-1 upregulation following p53 loss and cell transformation. *Oncogene* 31: 664–670, 2011.
49. Villablanca JG, London WB, Naranjo A, McGrady P, Ames MM, Reid JM, McGovern RM, Buhrow SA, Jackson H, Stranzinger E, Kitchen BJ, Sondel PM, Parisi MT, Shulkin B, Yanik GA, Cohn SL, and Reynolds CP. Phase II study of oral capsular 4-hydroxyphenylretinamide (4-HPR/fenretinide) in pediatric patients with refractory or recurrent neuroblastoma: a report from the Children's Oncology Group. *Clin Cancer Res* 17: 6858–6866, 2011.
50. Waak J, Weber SS, Gorner K, Schall C, Ichijo H, Stehle T, and Kahle PJ. Oxidizable residues mediating protein stability and cytoprotective interaction of DJ-1 with apoptosis signal-regulating kinase 1. *J Biol Chem* 284: 14245–14257, 2009.
51. Wilson MA. The role of cysteine oxidation in DJ-1 function and dysfunction. *Antioxid Redox Signal* 15: 111–122, 2010.
52. Wilson MA, Collins JL, Hod Y, Ringe D, and Petsko GA. The 1.1-A resolution crystal structure of DJ-1, the protein mutated in autosomal recessive early onset Parkinson's disease. *Proc Natl Acad Sci U S A* 100: 9256–9261, 2003.
53. Xu J, Zhong N, Wang H, Elias JE, Kim CY, Woldman I, Pifl C, Gygi SP, Geula C, and Yankner BA. The Parkinson's disease-associated DJ-1 protein is a transcriptional co-activator that protects against neuronal apoptosis. *Hum Mol Genet* 14: 1231–1241, 2005.
54. Yang B, Fan L, Fang L, and He Q. Hypoxia-mediated fenretinide (4-HPR) resistance in childhood acute lymphoblastic leukemia cells. *Cancer Chemother Pharmacol* 58: 540–546, 2006.
55. Ying M, Zhou X, Zhong L, Lin N, Jing H, Luo P, Yang X, Song H, Yang B, and He Q. Bortezomib sensitizes human acute myeloid leukemia cells to all-trans-retinoic acid-induced differentiation by modifying the RARalpha/STAT1 axis. *Mol Cancer Ther* 12: 195–206, 2013.
56. Zhang J, Cao J, Weng Q, Wu R, Yan Y, Jing H, Zhu H, He Q, and Yang B. Suppression of hypoxia-inducible factor 1alpha (HIF-1alpha) by tirapazamine is dependent on eIF2alpha phosphorylation rather than the mTORC1/4E-BP1 pathway. *PLoS One* 5: e13910, 2010.
57. Zhong N, Kim CY, Rizzu P, Geula C, Porter DR, Pothos EN, Squitieri F, Heutink P, and Xu J. DJ-1 transcriptionally upregulates the human tyrosine hydroxylase by inhibiting the sumoylation of pyrimidine tract-binding protein-associated splicing factor. *J Biol Chem* 281: 20940–20948, 2006.

58. Zhou W, Zhu M, Wilson MA, Petsko GA, and Fink AL. The oxidation state of DJ-1 regulates its chaperone activity toward alpha-synuclein. *J Mol Biol* 356: 1036–1048, 2006.

Address correspondence to:
Dr. Bo Yang
Zhejiang Province Key Laboratory
of Anti-Cancer Drug Research
Department of Pharmacology
College of Pharmaceutical Sciences
Zhejiang University
Zijin'gang Campus
Room 113
Hangzhou 310058
China

E-mail: yang924@zju.edu.cn

Date of first submission to ARS Central, May 23, 2013; date of final revised submission, December 30, 2013; date of acceptance, January 5, 2014.

Abbreviations Used

3-MA = 3-methyladenine
4-HPR = N-(4-hydroxyphenyl) retinamide
ASK1 = apoptosis signal-regulating kinase 1
DSS = disuccinimidyl suberate
FACS = fluorescence activated cell sorting
GSH = glutathione
JNK = c-Jun N-terminal kinase
LC-MS/MS = liquid chromatography-tandem mass spectrometry
MAP3K = MAP kinase kinase kinase
MAPK = mitogen-activated protein kinase
NAC = N-acetyl-L-cysteine
ROS = reactive oxygen species
RTV = relative tumor volume
SAPKs = stress-activated protein kinases
siRNA = small interfering RNA
T/C = RTV of treatment/RTV of control
Trx = thioredoxin